Design and assessment of a Solid-State Transformer built around a thin grain oriented electrical steel wound core

Houssam Ichou, Daniel Roger, Mathieu Rossi, Thierry Belgrand, Regis Lemaitre

Design and assessment of a Solid-State Transformer built around a thin grain oriented electrical steel wound core

Houssam Ichou[a,*], Daniel Roger[a], Mathieu Rossi[a], Thierry Belgrand[b] and Regis Lemaitre[b]

[a] Univ. Artois, EA4025, LSEE, 62400 Béthune, France
[b] thyssenkrupp Electrical Steel, 62330 Isbergues, France

ARTICLE INFO

Keywords:
Grain Oriented Electrical Steel
Medium Frequency Transformer
Solid-State Transformer
Thermal Model
Power converters
Loss estimation
Non-sinusoidal excitation

ABSTRACT

The increasing part of intermittent renewable energy requi res significant modifications of the electric grid. The introduction of smart nodes, where the power transfer can be adjusted in real time in addition to the classical voltage change and the galvanic isolation, becomes an important asset for the grid balance. Transformers associated to power electronic converters can ensure this function, they are known generically as Solid-State Transformers (SST). Their high specific power also opens opportunities for railway application. SSTs can work at high frequencies (a few tenth of kHz), with complex PWM topologies that generate complex waveforms approaching to sines, and transformers built with ferrite or nanocrystalline cores operating at low flux densities. The paper proposes a complementary approach that consists in using simple converters topologies working in square waves and transformers operating at medium frequencies (MF), around a few kHz and high flux densities. The cores are made of wound cores made of thin grain-oriented electrical steel (GOES). The proposed technology can be easily transposed to high powers units whilst maintaining a good technical-economic balance.

1. Introduction

The complexity of the electric grid has increased due to the growth of renewable energy sources (wind farms, photovoltaic plants, etc.). Solid State Transformers (SST) are relevant tools for ensuring proper monitoring of energy flows and flexible operation of the grid [1]. Classical SSTs are assemblies of power semiconductor switches, driving hardware and HF transformers. Several cells are associated for getting powers units. Each cell is bidirectional. SST cells using multi-level converters and transformers that operate at high frequencies have been developed [2, 3]. This concept can be used for Smart Grid applications [4] but also in other domains as renewable energy or railway traction [5]. The compactness, reliability and efficiency of SST are becoming higher and higher [6, 7]. The main challenges are high power density and reliability whilst maintaining a reasonable cost.

Grain-oriented electrical steel (GOES) cores is a complementary solution for designing high power SST cells, because they can operate at at very high flux densities and medium frequencies (few kHz). The central element is the medium frequency transformer (MFT), which is associated to basic and reliable converters operating in square waves. The design approach consists in finding the best possible balance between the wound core geometry, the winding design, the topology of the power electronic converters and the control laws. The MFT designed upon a wound magnetic core made of thin GOES sheets. With this structure, the magnetic field and the resulting polarisation are both in the GOES sheets rolling direction: the wound core can be used up to high flux densities levels because the saturation polarisation of the GOES is 2.03T; the operating flux density can reach 1.9T for conventional transformers but it must be slightly reduced with the increase in frequency. GOES has a mineral coating that can withstand temperatures up to (800°C). The core can work at temperatures up to (400°C) without any significant reduction in magnetisation capability [8]. At high temperature the natural increase in resistivity reduces the eddy currents losses. The paper deals with the design of a high-power SST cell based of a GOES wound core and standard IGBT converters with simple control strategies. With the proposed thermal management, the compact MFT operates at $1.6T$ and $2kHz$. The specific power is $2.2kW/kg$ with an efficiency of 96% for a $30kW$ SST cell.

2. SST Modular structure

Identical SST cells are assembled together to form high power SSTs. Each cell contains two reversible single-phase converters and a MFT ensuring the galvanic insulation and the voltage change. The cells are connected in series on the high voltage (HV) side and in parallel for the low voltage (LV) side as illustrated in Fig. 1. Each grid has a reference to ground for safety purposes. When the negative pole of the HV grid is grounded, Fig. 1 shows that the transformer of the upper cell has to withstand the full voltage of the HV grid between the primary winding, the secondary one and the core, which must be grounded (common mode insulation). The converters of the HV side must be placed in side an insulated rack able to withstand the common mode voltage. Their Boolean signals command must be transmitted by optical fibres in order to avoid disturbance of the control by leakage currents from the device to be controlled. Each cell is separately controlled to ensure the balance of the global system; the cell commands must obey a global control system imposing the voltages and the power transfer.

*First author
houssam.ichou@univ-artois.fr (H. Ichou)
ORCID(s): 0000-0003-4396-0952 (H. Ichou)

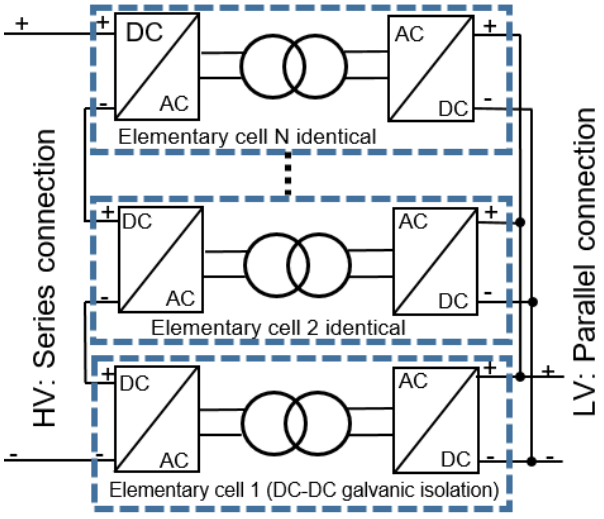

Figure 1: Modular structure of a high power SST.

3. Design of the MFT with a wound GOES core

The modular structure imposes a reinforcement of the common-mode insulation of the HV coil. The MFT is designed for a $30kV_{peak}$ common-mode maximum insulation voltage. The critical distances have been estimated using the Paschen curve of Fig 2 drawn for dry air at ambient temperature. At sea-level pressure ($10^5 Pa$), the estimation of distance that creates the ionisation of air between flat electrode that have a potential difference of $30kV_{RMS}$ is $12mm$. Safety margins are applied because the electric field lines in through air are not straight as in Paschen's experiences. The safety margin is larger for the critical distance between the coil and the core because of the presence of sharp angles. The critical distances defined in figure 3 are then set to $d_1 = 20mm$ and $d_2 = 18mm$.

The $0.18mm$ thick GOES sheets is wound on a mandrel of the specific shape and annealed. For the sake of winding insertion, the core is cut in two halves. The resulting pole faces have been worked out to ensure minimum air-gap ~~an~~ short circuits. Fig. 4 show be core before and after the cutting operation. Fig. 5 is a picture of the MFT. The size of the HV winding ~~is larger~~ (on the left leg) is larger than the LV one.

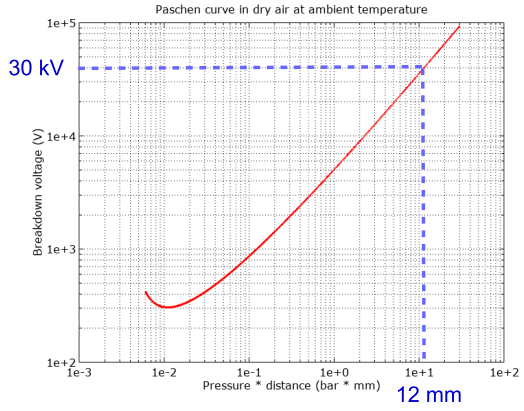

Figure 2: Paschen curve for dry air at room temperature.

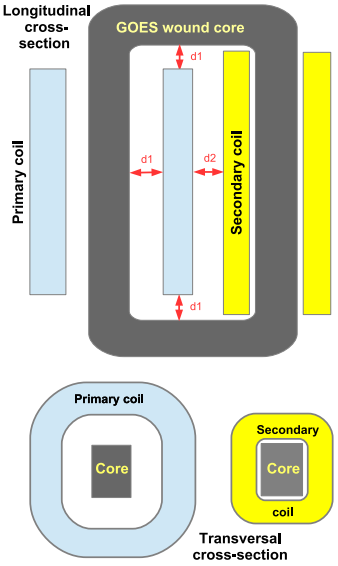

Figure 3: MFT topology with large distances of air around the HV coil for the common-mode insulation.

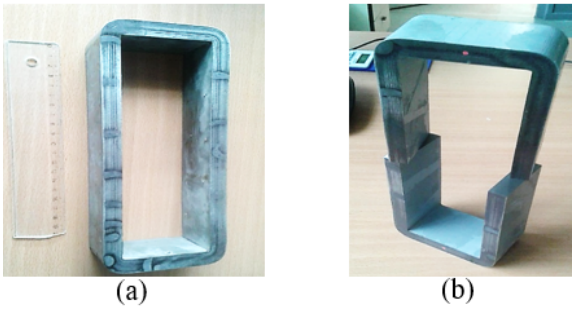

Figure 4: GOES wound core before and after the cutting process.

Figure 5: MFT with the common-mode insulation distances for the HV coil, the total weight is $14kg$.

4. Core losses

For designing the MFT, which is the central element of the SST cell, the core losses are of utmost importance. Experimental investigations are made at medium frequencies under the classical sine voltages under rectangular ones. The peak value of the flux density is the key point for comparing results.

~~The measurement procedure is classical (via Epstein frame) for measuring the magnetic properties of GOES. The secondary coil is used for measuring the voltage waveform and computing the flux in the core by integration.~~ The primary is fed by a voltage source; a broadband current probe measures the primary current waveform for computing the magnetic field in the core. Core losses are computed from the measurements at steady state.

The voltage source must have a strict null dc component. For rectangular waves the voltage source is a H-bridge inverter, which command is a micro controller that imposes strictly a 50.00% duty cycle. It uses high accuracy timers for avoiding any DC component. A low-pass LC filter in introduced between the H-bridge and the primary coil for getting a sine source of similar RMS voltage. The peak value of the flux density in the core is tuned by acting on the dc input voltage of the H-bridge inverter.

Fig. 6 shows that, for medium frequencies and for the same peak value of the flux density, the core losses are slightly lower in square wave than in sine wave. Fig. 7 shows that there is room for improvement in the manufacturing process going from the cut core to the completed transformer, this root causes are under investigation. The manufacturing process can be improved for higher frequencies.

5. Command of the SST cell

Fig. 8 gives details on the SST cell. The converters are H-bridges. When power is transferred from HV side to LV side, the first converter operates as an inverter producing a

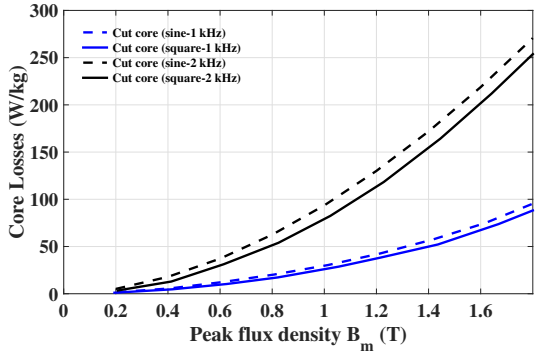

Figure 6: Core losses ~~in nude cores~~ for sine and square voltages.

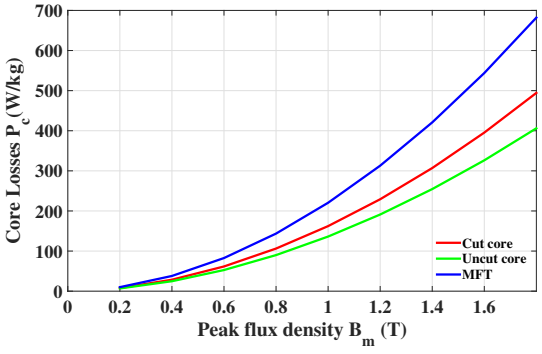

Figure 7: Core losses for square waves at $3kHz$ at the three steps of the manufacturing process.

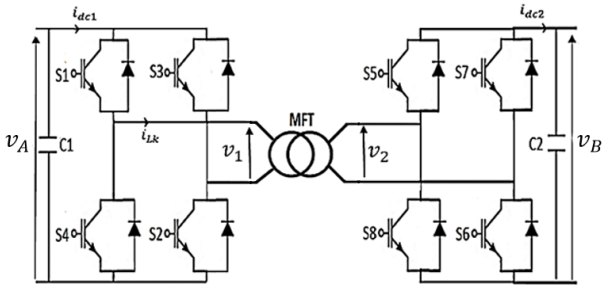

Figure 8: Detailed stricture of a SST cell.

rectangular voltage v_1 at a constant frequency. The second converter operates as a controlled rectifier. The symmetrical structure allows a power transfer in both directions, depending on the control strategy. [9, 10]. The simplified equivalent circuit of the cell, presented in Fig. 9, is established by neglecting the resistances. Sign conventions are chosen to have a positive power when the power flows from source V_A to source V_B. The transformer leakage inductance L_K ensures the basic rule of power electronics which prevents a short circuit between the two voltages sources v_1 and v_2 for Fig. 9; it makes possible the control of the instantaneous current i_{LK}.

One possible control strategy is presented in Fig. 10. The first inverter is commanded with Boolean signals for

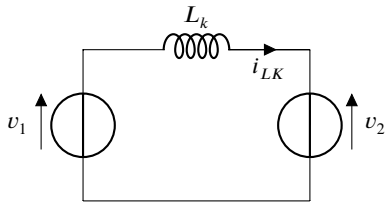

Figure 9: Simplified representation of the cell.

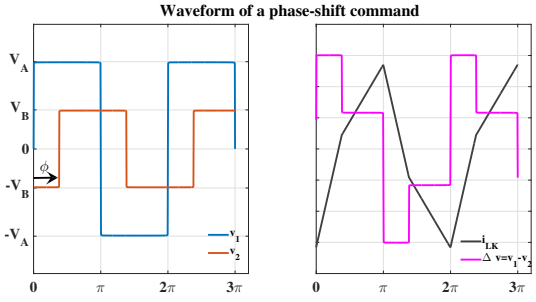

Figure 10: Voltage and current waveforms for a simple control strategy.

producing a square voltage v_1 with a duty cycle equal to 50%. the second inverter is also commanded for generating a rectangular voltage v_2 but with a phase-shift φ from the first one. This method, called "Phase-shift modulation"(PSM), has only one command parameter φ, defined between $-pi$ and $+pi$. Fig. 10 shows an example of the current i_{LK} waveform for a voltage across the inductance L_K imposed by the inverter commands. the current instantaneous value is given by (1). The men value of the transferred power transmitted from the source A to the source B is given by (2).

$$i_{LK} = \frac{1}{L_K}\int (v_1 - v_2)\, dt \tag{1}$$

$$P_{tr} = \frac{1}{T}\int_0^T (v_1.i_{LK})\, dt = \frac{V_A V_B}{\omega L_K \pi}\varphi(\pi - \mid \varphi \mid) \tag{2}$$

The sign of the control parameter φ defines the direction of power transfer and its value. The Fig. 11 shows the power transmitted as a function of the phase-shift φ. The transmitted power has extremes for a certain value of φ; the maximum power is reached for $\partial P_{tr}/\partial P_{trmax} = 0$ with :

$$P_{trmax} = \frac{V_A V_B}{8.L_K.f} \tag{3}$$

The maximum power is obtained for $\varphi = \pm\frac{\pi}{2}$.

5.1. MFT thermal model

The rated power of the MFT depends on the frequency f, the peak flux density B_m and the winding maximum temperature, which is imposed by the technology of their electrical insulation system (EIS) (IEC 62114). For standard organic insulation technologies made with polymers, the maximum temperature is defined by the thermal class of the EIS, which is the operating temperatre that corresponds to a life expectancy of 20000h. The most common classes are F (155°C), H (180°C), and C (200°C). Consequently for getting a high specific power, the thermal management is essential. The MFT is placed vertically in a forced air flow imposed by a fan located under the transformer.

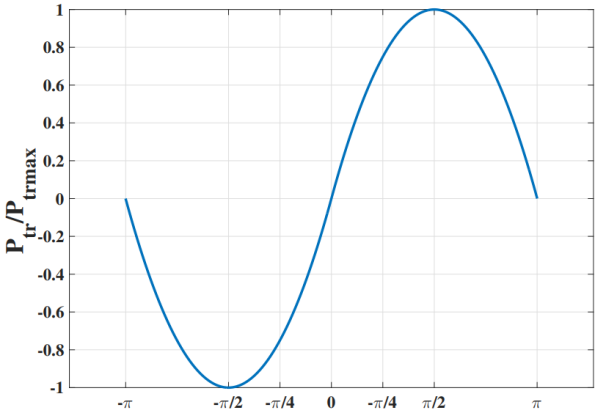

Figure 11: Power transmitted as a function of phase-shift φ.

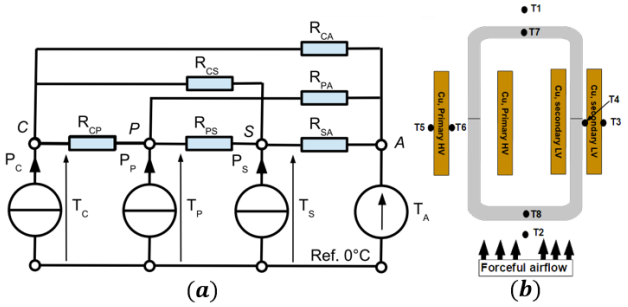

Figure 12: (a): Thermal model ; (b): Thermocouples positions.

A thermal model considering this thermal management is essential for estimating the temperature of each part of the MFT in any operating conditions. The rated power is obtained when the thermal limit of the weakest part is reached. The steady-state thermal model is shown in Fig. 12a based on three assumptions:

(1) The are uniformly distributed in the volume of the element under consideration.
(2) the temperature is supposed uniform in a part of the MFT, with this hypothesis the simpplified equivalent thermal circuit is made on ony 4 nodes one for each coil, one for the transformer core and one for the ambient airflow.
(3) Thermal resistances of the model are independent of temperature (linear model).

For estimating the thermal resistances of the model, thermocouples are placed in different parts of the transformer as shown in Fig. 12b. Experiments are made considering three

independent test conditions: No-load; DC current in the primary coil DC current in the secondary coil. Results at steady state are presented in Table 1.

Table 1
Temperature of model nodes at steady states.

	No-load test $f = 3kHz$ $P_c = 351.24W$	DC supply HV side $P_p = 56.26W$	DC supply LV side $P_s = 42.06W$
$T1$ (°C)	23.95	24.3	22
$T2$ (°C)	22.75	22	21
$T3$ (°C)	69.35	23.2	40.52
$T4$ (°C)	80.65	23.35	41.65
$T5$ (°C)	61.9	32.95	22.40
$T6$ (°C)	69.15	35.3	22.55
$T7$ (°C)	128.8	26.4	23.9
$T8$ (°C)	121.65	25.9	22.42

The nodes T_P, T_s, T_c and T_a are the average temperature of the primary winding ($T5, T6$), the secondary winding ($T3, T4$), the core ($T7, T8$) and the ambient air ($T1, T2$). The power sources P_P, P_s and P_c represent the losses in the primary, secondary windings and core respectively. Thermal resistances represent the thermal transfers between each part of the MFT. The model can be described by (4).

$$P_{loss} = AT - BT_a \tag{4}$$

$$\text{With : } P_{loss} = \begin{bmatrix} P_c \\ P_p \\ P_s \end{bmatrix}; T = \begin{bmatrix} T_c \\ T_p \\ T_s \end{bmatrix}; B = \begin{bmatrix} \frac{1}{R_{CA}} \\ \frac{1}{R_{PA}} \\ \frac{1}{R_{SA}} \end{bmatrix}$$

$$A = \begin{bmatrix} \frac{1}{R_{CS}} + \frac{1}{R_{CA}} + \frac{1}{R_{CP}} & \frac{-1}{R_{CP}} & \frac{-1}{R_{CS}} \\ \frac{-1}{R_{CP}} & \frac{1}{R_{CP}} + \frac{1}{R_{PA}} & 0 \\ \frac{-1}{R_{CS}} & 0 & \frac{1}{R_{CS}} + \frac{1}{R_{SA}} \end{bmatrix}$$

Three measurement tests have been evaluated to find the thermal model resistances, by fixing a power source and measuring the temperatures in different parts of the MFT by thermocouples. The open-circuit test shows the influence of P_c; the influence of P_P and P_s are determined by (DC supply of the corresponding winding). The thermal resistances measured on the prototype MFT are: $R_{CA} = 8.84°C/W$; $R_{PA} = 0.54°C/W$; $R_{SA} = 0.19°C/W$; $R_{CP} = 0.77°C/W$ and $R_{CS} = 0.19°C/W$.

The `table1` shows the temperatures measured by thermocouples at steady states from the three tests.

The temperatures of the different parts of the transformer

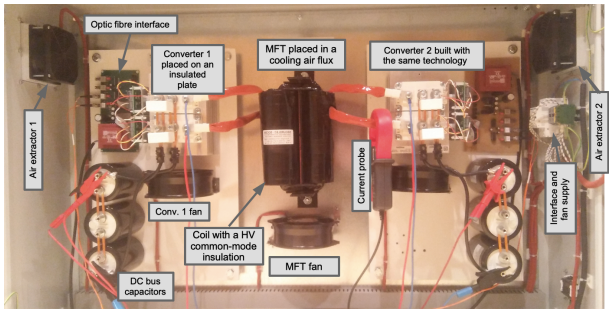

Figure 13: The experimental set-up of a SST cell.

are estimated by (5).

$$T = A^{-1}.(P_{loss} + B.T_a) \tag{5}$$

The Table 2 gives two examples of the possible performance of the prototype cell at two frequencies. The input data are the frequency and power transmitted by the cell, they allow to calculate the currents and to estimate the losses in the windings. Core losses are the result of measurements on the MFT at different frequencies and peak flux density. The temperatures are calculated with (5). The efficiency calculation takes into consideration the losses in the electronic converters.

Table 2
Estimation of temperatures in the MFT and cell efficiency for two operating point.

Frequency (kHz)	2	3
Power (kW)	30	40
T_c (°C)	224	261
T_p (°C)	146	171
T_s (°C)	142	170
Efficiency (%)	95.7	95.9

This result shows that the first operating point ($1.6T$, $2kHz$, $30kW$) allows to use class F coils with a safety margin of 9°C and that it is possible to increase the specific power and efficiency by the second operating point ($1.2T$, $3kHz$, $40kW$) using the class H coils. This approach, using conventional winding technology, shows that the ~~efficiJency~~ of the complete cell can be suitable when working with a hot wound core, provided that a large part of the power passes through the small volume of the MFT.

A $800V/800V$ SST cell prototype with a hot GO wound core has been built (Fig. 13). The primary H bridge is made of 2 standard $1200V/400A$ IGBT legs powered by a $800V$ DC voltage source. Experimental measurements in high power is in progress, in parallel with the construction of a second A $2.5kV/800V$ SST cell which will be the subject of an association of two SST cells.

6. Conclusion

The design of a SST cell aimed at providing a good technical economic balance has been presented, using a grain-oriented electrical steel wound core. The PSM method has shown better performance compared to complex PWM waveforms, which requires working with a rectangular waveform. With a wound magnetic core made of GOES ($0.18mm$) and conventional winding insulation systems, it is possible to build high-power SST cells. The thermal balance of the transformer must be carefully calculated and the leakage inductance reduced, while exploiting the good performance of grain-oriented electrical steel at high temperatures. This experimental study has been performed with a transformer of classical structure in terms of core arrangement and windings.

These results open up prospects for the design of compact hot wound core transformers by acting on the elements of the thermal model. It is possible to modify the transformer design to limit heat flows between the core and the windings and cooling them directly. This work is currently underway in parallel with the development of the regulations required to assemble the elementary cells to form a very high-power SST.

Acknowledgment

This work is funded by ThyssenKrupp Electrical Steel.

References

[1] J. E. Huber and J. W. Kolar, "Volume/weight/cost comparison of a 1mva 10 kv/400 v solid-state against a conventional low-frequency distribution transformer," in *2014 IEEE Energy Conversion Congress and Exposition (ECCE)*. IEEE, 2014, pp. 4545–4552.

[2] D. S. Oliveira, D. d. A. Honório, L. H. S. Barreto, P. P. Praça, A. Kunzea, and S. Carvalho, "A two-stage ac/dc sst based on modular multilevel converterfeasible to ac railway systems," in *2014 IEEE Applied Power Electronics Conference and Exposition-APEC 2014*. IEEE, 2014, pp. 1894–1901.

[3] M. Glinka and R. Marquardt, "A new ac/ac multilevel converter family," *IEEE Transactions on Industrial Electronics*, vol. 52, no. 3, pp. 662–669, 2005.

[4] F. Vaca-Urbano and M. S. Alvarez-Alvarado, "Power quality with solid state transformer integrated smart-grids," in *2017 IEEE PES Innovative Smart Grid Technologies Conference-Latin America (ISGT Latin America)*. IEEE, 2017, pp. 1–6.

[5] C. Zhao, D. Dujic, A. Mester, J. K. Steinke, M. Weiss, S. Lewdeni-Schmid, T. Chaudhuri, and P. Stefanutti, "Power electronic traction transformer—medium voltage prototype," *IEEE Transactions on Industrial Electronics*, vol. 61, no. 7, pp. 3257–3268, 2013.

[6] D. Dujic, F. Kieferndorf, and F. Canales, "Power electronic transformer technology for traction applications–an overview," *Electronics*, vol. 16, no. 1, pp. 50–56, 2012.

[7] K. Wang, Q. Lei, and C. Liu, "Methodology of reliability and power density analysis of sst topologies," in *2017 IEEE Applied Power Electronics Conference and Exposition (APEC)*. IEEE, 2017, pp. 1851–1856.

[8] M. Ababsa, O. Ninet, G. Velu, and J. Lecointe, "High-temperature magnetic characterization using an adapted epstein frame," *IEEE Transactions on Magnetics*, vol. 54, no. 6, pp. 1–6, 2018.

[9] Z. Haihua and A. M. Khambadkone, "Hybrid modulation for dual active bridge bi-directional converter with extended power range for ultracapacitor application," in *2008 IEEE Industry Applications Society Annual Meeting*. IEEE, 2008, pp. 1–8.

[10] B.-J. Byen, K.-P. Kang, Y. Cho, and A. Yoo, "A high-efficiency variable modulation strategy for a dual-active-bridge converter with a wide operating range," in *2015 9th International Conference on Power Electronics and ECCE Asia (ICPE-ECCE Asia)*. IEEE, 2015, pp. 240–245.

Houssam Ichou received his master degree in physics and energy engineering from the university of Paris-Saclay in 2016. In 2017 he joined the Electrotechnical Systems and Environment Laboratory (LSEE) of the University of Artois in Bethune (France) as an engineer. Currently, he is a doctoral student in the department of electrical engineering at the university of Artois, Bethune, France. Research deals with the study and design of a high-power solid-state transformer operating at medium frequency, intended for railway traction, using a thin grain oriented electrical steel. His research interests include magnetic material, power electronics, converter typologies and control systems.